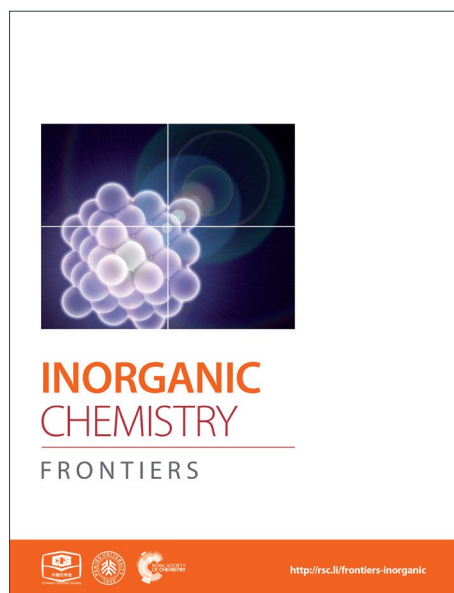
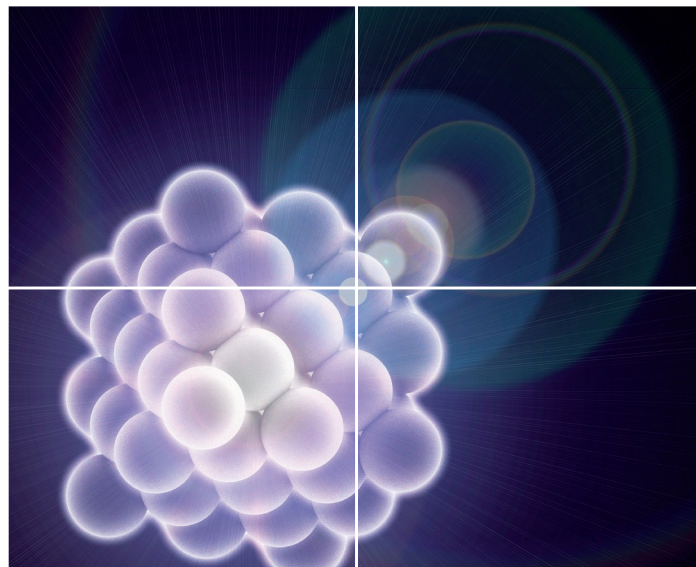


INORGANIC CHEMISTRY

FRONTIERS

Accepted Manuscript



This is an *Accepted Manuscript*, which has been through the Royal Society of Chemistry peer review process and has been accepted for publication.

Accepted Manuscripts are published online shortly after acceptance, before technical editing, formatting and proof reading. Using this free service, authors can make their results available to the community, in citable form, before we publish the edited article. We will replace this *Accepted Manuscript* with the edited and formatted *Advance Article* as soon as it is available.

You can find more information about *Accepted Manuscripts* in the [Information for Authors](#).

Please note that technical editing may introduce minor changes to the text and/or graphics, which may alter content. The journal's standard [Terms & Conditions](#) and the [Ethical guidelines](#) still apply. In no event shall the Royal Society of Chemistry be held responsible for any errors or omissions in this *Accepted Manuscript* or any consequences arising from the use of any information it contains.

RESEARCH ARTICLE

An outstanding Second-Harmonic Generation Material BiB₂O₄F: Exploiting the Electron-withdrawing Ability of Fluorine

Cite this: DOI: 10.1039/x0xx00000x

Received 00th January 2012,

Accepted 00th January 2012

DOI: 10.1039/x0xx00000x

www.rsc.org/

Rihong Cong,^{a*} Ying Wang,^a Lei Kang,^{b,c} Zhengyang Zhou,^a Zheshuai Lin,^{b*} and Tao Yang^{a*}

It is well known that the incorporation of fluorine usually blue-shifts the absorption edge of a crystal due to the large electronegativity. Herein, we validate the new functionality of fluorine that leads to the strong second harmonic generations (SHG) effect in a unique nonlinear optical (NLO) bismuth borate, BiB₂O₄F, where F coordinates to both B³⁺ and Bi³⁺ cations. The F-incorporation would not only form a more asymmetric unit [BO₃F], comparing to the almost optical isotropic [BO₄], but also withdraw the non-bonding electrons of Bi³⁺, increasing its local polarization, thus the total SHG efficiency would be increased significantly. Indeed, experimental measurements and first-principles calculations both support our anticipation that BiB₂O₄F is a phase-matchable NLO material with the exceptional large SHG response. In order to further consolidate the functionality of fluorine, a comparison study with the structural-similar compound BiB₂O₄(OH) was performed.

Introduction

Metal borates are well-known candidates for ultraviolet (UV) nonlinear optical (NLO) materials because of their tremendous structure flexibility and outstanding intrinsic physical characteristics, such as high thermal stability and good transparency in UV region.¹⁻³ Usually, a noncentrosymmetric structure consisting of asymmetric or polar structural unit exhibits a large second harmonic generation (SHG) response.^{4,5} For example, the large SHG effect for β-BaB₂O₄ and LiB₃O₅ are mainly contributed by the planar polyanions [B₃O₆]³⁻ and [B₃O₇]⁵⁻, respectively.^{6,7} Meanwhile, the metal-centered MO_x polyhedra could also have a substantial or even major contribution to the SHG efficiency. Here, *M* could be cations with second-order *Jahn-Teller* distortion, such as *d*⁰, *d*¹⁰ cations showing a polar displacement in an octahedral coordination,⁸⁻¹¹ or *p*-block cations with stereochemical lone pair electrons (i.e. Pb²⁺ and Bi³⁺).¹²⁻¹⁴ Apparently, a combination of above-mentioned functional units can lead to a synergic effect, achieving excellent SHG properties, like Cd₄BiO(BO₃)₃, which shows an SHG response about six times that of KH₂PO₄ (6 × KDP).¹¹ Pb₂B₅O₉I is another representative showing a promising SHG performance arisen from all three components, Pb²⁺ cation, I⁻ anion, and the polyborate anion.¹⁵

It is known that the introduction of halogen atoms into metal borates is beneficial to the transparency in UV-region,¹⁶ such as KB₂B₃O₇F (KBBF).¹⁷ Generally, F can be either coordinated to metal cations (forming M-F bonds) or boron

atoms (forming B-F bonds, e.g. in [BO₃F]⁴⁻ group). The former is quite usual, like KBBF,¹⁸ Pb₃B₆O₁₁F₂,¹⁹ and Cd₅(BO₃)₃F.²⁰ However, the borates containing B-F bonds are rare; BaBOF₃ was the first reported example,²¹ and followed by Na₃B₃O₃F₆,²² Li₂B₆O₉F₂,²³ Li₂B₃O₄F₃,²⁴ and LiB₆O₉F.²⁵ Because fluorine atom is more electronegative than oxygen atom, it is expectable that [BO₃F] is more asymmetric than [BO₄] unit. In fact, most of above mentioned fluoroborates are show observable SHG effects.^{18,19,20,26}

Is there another way to further enhance the SHG response rather than merely superimposing polarizations from individual functional units? Our idea is to take full advantage of the electron-withdrawing ability of F atom, not only creating an asymmetric structural unit ([BO₃F]) but also enhancing the local polarization of Bi³⁺ cations. BiB₂O₄F is a unique fluoroborate that F coordinates to both boron and bismuth.²⁷ It crystallizes in the space group *P*3₂ as shown in Fig. 1a, however it was previously reported as a moderate SHG material (about 1.8 × KDP), which is apparently lower than our expectation. In order to clarify this discrepancy, herein we present a re-investigation of the SHG property of BiB₂O₄F by both theoretical and experimental methods. Our first-principles calculations suggested a very strong SHG effect in BiB₂O₄F (> 10 × KDP), which was further validated by the re-measured optical properties. Furthermore, the comparison of the SHG properties between BiB₂O₄F and its structural similar

compound $\text{BiB}_2\text{O}_4(\text{OH})$ help us to understand the function of F in NLO materials.

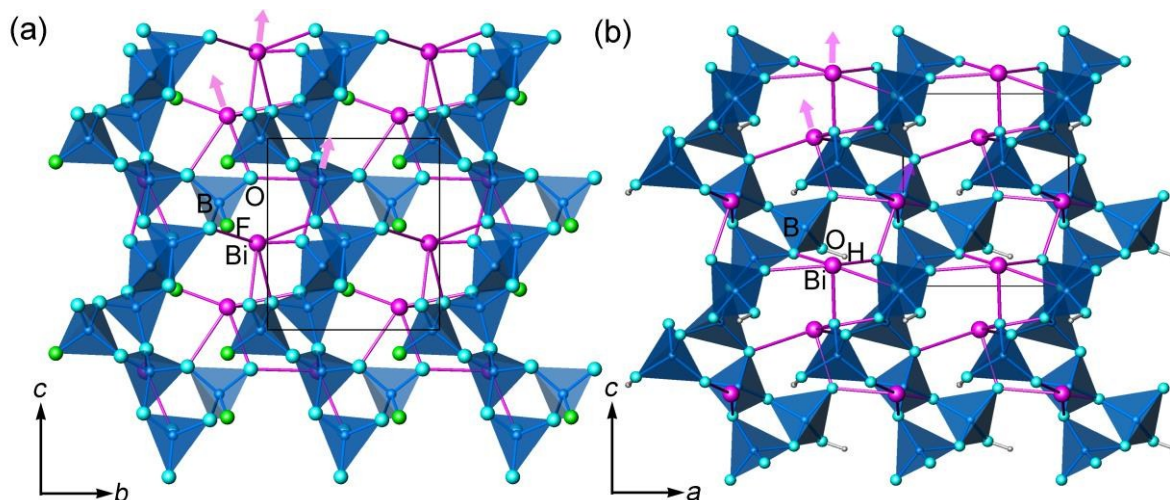


Fig. 1 Projection of the structures of (a) $\text{BiB}_2\text{O}_4\text{F}$ and (b) $\text{BiB}_2\text{O}_4(\text{OH})$ along the [100] and [010] directions respectively. The pink arrows imply the orientation of lone pair electrons on Bi^{3+} cations. The unit cells are indicated by the black boxes.

Experimental

Synthesis

Typically, to obtain $\text{BiB}_2\text{O}_4\text{F}$ crystals, a mixture of 0.3638 g $\text{Bi}(\text{NO}_3)_3 \cdot 5\text{H}_2\text{O}$, 0.9275 g H_3BO_3 and 0.0630 g NaF with Bi/B/F ratio of 1/20/2 was charged into the autoclave with additional 0–0.5 mL of water. The autoclave was sealed and heated at 200 °C for 3 days. After reaction, the product was washed by distilled water, and colorless crystals of $\text{BiB}_2\text{O}_4\text{F}$ with a yield of ~90% (based on Bi) were obtained. For the synthesis of $\text{BiB}_2\text{O}_4(\text{OH})$ (yield: ~90%), a mixture of 0.3495 g Bi_2O_3 and 1.855 g H_3BO_3 with Bi/B ratio of 1/20 was ground in an agate mortar, and then transferred into a 25 mL Teflon autoclave, which was sealed and heated at 220 °C for 3 days after adding 2 mL of water.

The use of bismuth source, NaF and appropriate amount of water strongly affected the final product. For example, the employment of $\text{Bi}(\text{NO}_3)_3 \cdot 5\text{H}_2\text{O}$ as bismuth source together with appropriate amount of NaF are necessary for the synthesis of $\text{BiB}_2\text{O}_4\text{F}$. $\text{BiB}_2\text{O}_4(\text{OH})$, on the other hand, can only be synthesized by using Bi_2O_3 as bismuth source, and the purity of product was sensitive to the content of water. If the added water was between 1 and 3 mL, pure $\text{BiB}_2\text{O}_4(\text{OH})$ can be obtained; if less than 1 mL, $\text{Bi}[\text{B}_4\text{O}_6(\text{OH})_2]\text{OH}$ appeared as impurity; if more than 3 mL, a mixture of $\text{BiB}_2\text{O}_4(\text{OH})$ and $\text{Bi}_3\text{B}_5\text{O}_{12}$ formed. Here the purity of as-made $\text{BiB}_2\text{O}_4\text{F}$ and $\text{BiB}_2\text{O}_4(\text{OH})$ was verified by powder X-ray diffraction (see details in the Electronic Supplementary Information (ESI)). Only phase-pure samples were used for further characterizations.

Structure Analysis and Characterizations

Single-crystal X-ray diffraction (XRD) data was collected on a Super Nova-CCD using graphite-monochromated Mo K α radiation ($\lambda = 0.71073 \text{ \AA}$) at 104 K. Powder XRD data were collected to confirm the phase purity on a PANalytical X'pert

diffractometer with a PIXcel 1D detector (Cu K α , 40 kV and 40 mA). Thermogravimetric analysis (TG) was performed on a Mettler-Toledo TGA/DSC instrument under a N_2 flow. The UV-Vis diffuse reflectance spectra were recorded at room temperature using a powder sample with BaSO_4 as a standard (100% reflectance) on a Shimadzu UV-3100 spectrophotometer. Reflectance spectra were converted to absorbance spectra using the Kubelka-Munk function. The electronic structures and SHG coefficients for $\text{BiB}_2\text{O}_4\text{F}$ and $\text{BiB}_2\text{O}_4(\text{OH})$ were calculated using the first-principles plane-wave pseudopotential method implemented in the CASTEP program.^{28,29} Details of the computational method are given in the ESI.

Powder SHG signals were measured using the experimental method adapted from Kurtz and Perry.³⁰ Samples of $\text{BiB}_2\text{O}_4\text{F}$ and $\text{BiB}_2\text{O}_4(\text{OH})$ were ground and sieved into different particle sizes. As a reference, crystalline $\alpha\text{-BiB}_3\text{O}_6$ (BIBO) sample was ground into the range of 105–125 μm . The powder sample was pressed between quartz slides and secured with a tape in 1 mm thick aluminum holder, which has a $\Phi 8 \text{ mm}$ hole. The holder was then irradiated with a pulsed infrared beam (970 mV, 10 ns, 1 Hz, 18 mW/cm²) from a Q-switched YAG:Nd³⁺ laser of wavelength 1064 nm. A cutoff filter was used to minimize the background, and an interference filter ($530 \pm 10 \text{ nm}$) was used to select the second harmonic for detection with a photomultiplier tube attached to an oscilloscope. This procedure was then repeated using BIBO (as a standard). No index-matching fluid was used in any of the experiments.

Results and Discussion

Structural and electronic Characteristics

In literature, the crystal structure of $\text{BiB}_2\text{O}_4\text{F}$ was solved by powder XRD technique convincingly in the space group $P3_2$ ($a = 6.7147(1) \text{ \AA}$ and $c = 6.4688(1) \text{ \AA}$).²⁷ Our hydrothermal synthesis leads to aggregated particles in tens of micrometers and the EDX analysis on a selected area confirms the existence

of fluorine in the compound (see Fig. 2). As shown in Fig. 1a, helical borate chains in $\text{BiB}_2\text{O}_4\text{F}$, which is constructed by corner-shared borate tetrahedra ($2\text{BO}_4 + \text{BO}_3\text{F}$), are interconnected by Bi^{3+} to form a three-dimensional condensed structure.

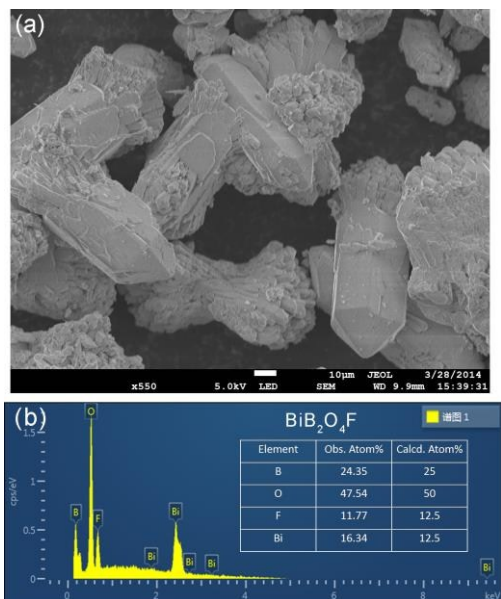


Fig. 2 (a) SEM image and (b) EDX results for $\text{BiB}_2\text{O}_4\text{F}$. The observed atomic ratio was presented, which is consistent with the calculated value within the experimental error.

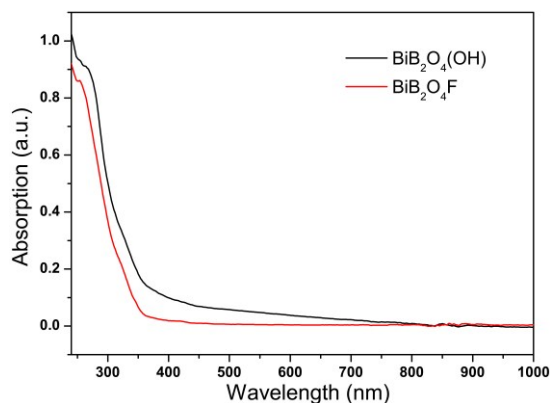


Fig. 3 UV-Vis-NIR absorption spectra for $\text{BiB}_2\text{O}_4\text{F}$ and $\text{BiB}_2\text{O}_4(\text{OH})$.

In the same article reporting $\text{BiB}_2\text{O}_4\text{F}$,²⁷ there was another compound with the formula “ $\text{Bi}_3[\text{B}_6\text{O}_{13}(\text{OH})]$ ”, possessing highly related structure with $\text{BiB}_2\text{O}_4\text{F}$. It was also solved by powder XRD technique but in a very low symmetry, i.e. triclinic. In ref. 27, the authors claimed that the triclinic structure was a tentative (probably inaccurate) model, and during the structure refinements with powder XRD data, constraints were applied to get reasonable structure parameters. An exact structure determination needs the single crystal X-ray diffraction. Moreover, it was also suspicious about the formula “ $\text{Bi}_3[\text{B}_6\text{O}_{13}(\text{OH})]$ ”, because the TG weight loss observed in ref. 27 and herein our work is 2.5 and 2.77 wt% (Fig. S1 in ESI), respectively, which is more consistent with the formula

$\text{BiB}_2\text{O}_4(\text{OH})$ (calcd. 2.9 wt%) rather than $\text{Bi}_3[\text{B}_6\text{O}_{13}(\text{OH})]$ (calcd. 1.0 wt%).

We made our efforts to the syntheses and obtained small single crystals of “ $\text{Bi}_3[\text{B}_6\text{O}_{13}(\text{OH})]$ ”, thus a single crystal XRD become possible. More than a dozen of single crystals were selected for XRD data collection, in most cases, the R_{int} values are quite high (>0.20), either using a triclinic or trigonal symmetry during the manual data reduction. We speculate that the very large absorption of Bi^{3+} to X-ray is the possible cause, especially in the case that the spatial density of Bi^{3+} in $\text{BiB}_2\text{O}_4(\text{OH})$ is very high.

Fortunately, we eventually obtained a suitable dataset by cracking the large crystal into pieces, and selecting a small fraction for data collection at 104 K. Even though, only Bi^{3+} could be refined anisotropically, while other light atoms (boron and oxygen) were refined isotropically. The obtained atomic coordinates were chemically reasonable with regular bond distances. The final crystal structure was refined in the polar space group $P3_1$ by full-matrix least-squares refinement.³¹ Detailed crystallographic information is listed in Table S1. The atomic coordinates and selected bond lengths are listed in Table S2 and S3, respectively. CIF file and details of the structure are also provided in ESI. However, there are still small residual electron densities around Bi^{3+} , which was therefore not surprising in such a case. In overall, the currently $P3_1$ and the previously reported $P1$ structures are basically the same, except a small difference in formula and the coordination of some of the boron. In fact, the higher symmetry in $P3_1$ leads to much less structural parameters, which gave a green light for DFT calculations.

For $\text{BiB}_2\text{O}_4(\text{OH})$, there are 8 crystallographically independent non-hydrogen atoms, including 1 Bi, 2 B, and 5 O (shown in Fig. 1b). All atoms locate at general positions. Coordinates for H were determined based on structural analysis and bond valence sum (BVS) calculations. Both B are coordinated by four oxygen atoms in regular tetrahedral environments. The structure of $\text{BiB}_2\text{O}_4(\text{OH})$ is very similar with $\text{BiB}_2\text{O}_4\text{F}$, the main difference is the replacement of F^- by OH^- , as shown in Fig. 1. Clarifying the structure similarity between $\text{BiB}_2\text{O}_4\text{F}$ and $\text{BiB}_2\text{O}_4(\text{OH})$ would facilitate our further discussion about the structure-property relationship (shown later).

The bandgap energies for $\text{BiB}_2\text{O}_4\text{F}$ and $\text{BiB}_2\text{O}_4(\text{OH})$ were estimated to be 4.43 and 4.28 eV, respectively, by the maximum peak of the first order differential curve for UV-Vis-NIR absorption spectra (see Fig. 3). No obvious absorption in the range of 350-1000 nm indicates the transparency for both samples in the entire visible region.

The calculated electronic band structure of $\text{BiB}_2\text{O}_4\text{F}$ along the symmetry lines in the Brillouin zone of the unit cell is plotted in Fig. 4a. This structure has an indirect bandgap (3.36 eV) which is smaller than the experimental value (4.43 eV) due to the discontinuity of XC energy. Fig. 4b gives the total and partial density of states (DOS and PDOS) projected on the constituent atoms in $\text{BiB}_2\text{O}_4\text{F}$. Several electronic characteristics considering the respective groups can be summarized as

follows: (i) the energy region below -10 eV is mainly composed of the isolated inner orbitals of Bi ($5d$), O ($2s$), and F ($2s$), which are strongly localized deeply in the valence band (VB) and have a negligible influence with the neighbor atoms; (ii) the upper VB (from -10 eV) shows large hybridization between B ($2p$) and O/F ($2p$) orbitals, but the top of the VB is mainly composed of O ($2p$) orbitals, which is similar with the situation in BIBO;¹² (iii) the bottom of conduction band (CB) is mostly contributed by the orbitals of Bi ($6p$), O ($2p$). It should be emphasized that the states on both sides of the band gap are mainly composed of the orbitals from [BiO₅].

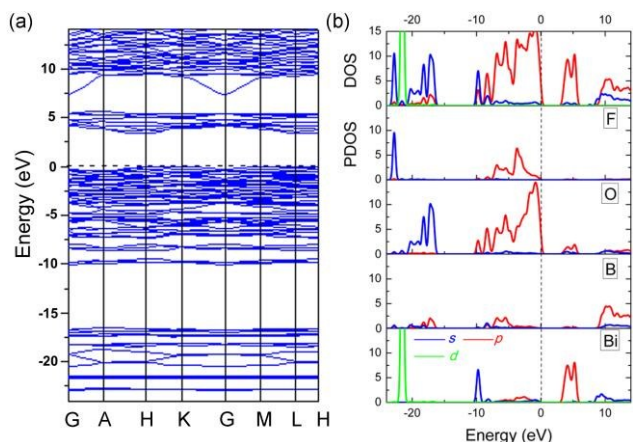


Fig. 4 Electronic structure in BiB₂O₄F (a) electronic band structure and (b) DOS/PDOS.

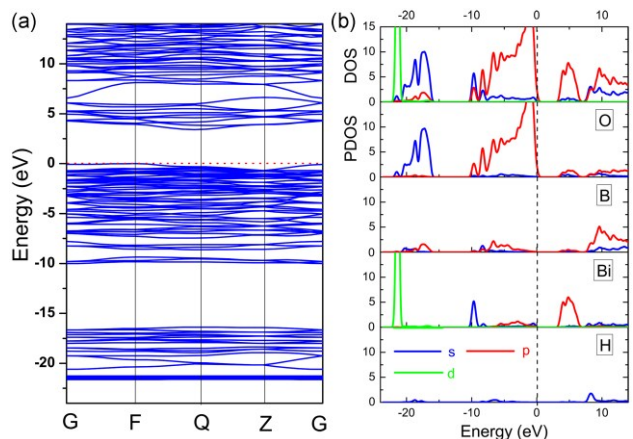


Fig. 5 Electronic structure in BiB₂O₄(OH) (a) electronic band structure and (b) DOS/PDOS.

Similar to BiB₂O₄F, the electronic band structure, DOS and PDOS of BiB₂O₄(OH) are shown in Fig. 5. The theoretical energy bandgap is calculated to be 3.41 eV (indirect gap). The top of the VB is mainly composed of O ($2p$) orbitals and the bottom of CB is mainly contributed by Bi ($6p$) and O ($2p$) orbitals, which are similar with the case in BiB₂O₄F. Additionally, the H $1s$ orbitals have hybridization with the

electronic states on the O atoms due to the formation of hydroxyl groups, but have a rather small contribution to both VB and CB. Therefore, one can easily find that the [BiO₅] group is also the major functional group in BiB₂O₄(OH).

Optical properties relevant to SHG output

The calculated linear refractive indices and birefringence for BiB₂O₄F and BiB₂O₄(OH) at 1064 nm are listed in Table 1. The birefringence values are a bit small, but still satisfy the phase-matching requirement for the SHG output in the IR and visible spectral region. Since the space group is $P3_2/P3_1$, there are four independent non-zero SHG coefficients due to the Kleinman symmetry relation, as shown in Table 1. The calculated SHG coefficients of BiB₂O₄F are much higher than that of BiB₂O₄(OH), and the values of d_{33} are significantly larger than other d_{ij} coefficients, which are -11.43 and -5.23 pm/V for BiB₂O₄F and BiB₂O₄(OH) respectively. Moreover, it is interesting that these values for BiB₂O₄F are even larger than the d_{ij} values of BIBO (expt. $d_{22}=2.53$ pm/V, $d_{16}=2.8$ pm/V, $d_{14}=2.4$ pm/V, $d_{23}=-1.3$ pm/V),³² which is known as a promising SHG material in borates. Consequently, the powder SHG coefficients for BiB₂O₄F and BiB₂O₄(OH) are estimated to be 5.82 and 3.62 pm/V according to the Kurtz-Perry method,³⁰ which are ~ 1.77 and 1.10 times of BIBO ($d_{\text{powder}} = 3.28$ pm/V, $\sim 8 \times$ KDP).

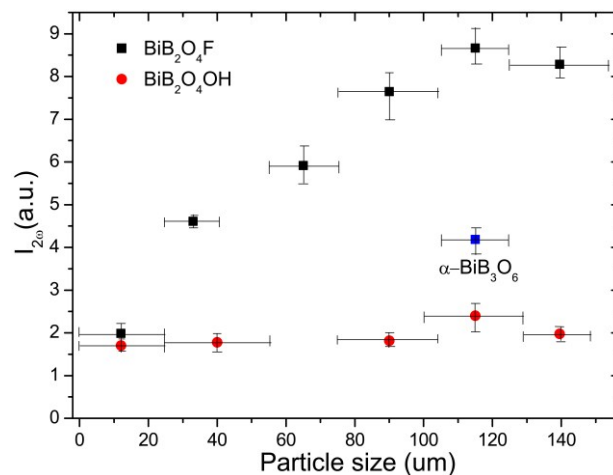


Fig. 6 Dependence of the measured powder SHG signals intensity with the particle size of BiB₂O₄F and BiB₂O₄(OH) (α -BiB₃O₆ as a reference).

Apparently, the theoretical calculations suggest excellent NLO performances for both of BiB₂O₄F and BiB₂O₄(OH). In order to verify the calculations, the powder SHG effects of BiB₂O₄F and BiB₂O₄(OH) were re-measured by Kurtz and Perry method, despite that they were previously reported to be

RESEARCH ARTICLE

Table 1 Calculated refractive index, birefringence, and SHG/PSHG effect in BiB₂O₄F and BiB₂O₄(OH), and the experimental PSHG effect as a comparison.

	Calculated refractive index n and birefringence Δn at 1064 nm			Calculated SHG coefficients	PSHG effect d_{powder}	
	n_o	n_e	Δn	d_{ij} (pm/V)	Cal.	Exp.
BiB ₂ O ₄ F	2.0699	2.0979	0.028	$d_{11} = -d_{12} = 4.49$; $d_{16} = -d_{22} = 2.28$ $d_{15} = d_{24} = 1.44$ $d_{33} = -11.60$	5.82 1.77*BIBO [#]	4.72 1.44*BIBO [#]
BiB ₂ O ₄ (OH)	2.1670	2.1403	0.027	$d_{11} = -d_{12} = 2.82$; $d_{16} = -d_{22} = 3.10$ $d_{15} = d_{24} = 0.16$ $d_{33} = -5.23$	3.62 1.10*BIBO [#]	2.48 0.76*BIBO [#]

[#] Powder SHG effect in BIBO is about 8×KDP (about 3.28 pm/V), from Ref. [32].

moderate in literature.²⁷ It should be noted that a low stability under laser irradiation was observed during the SHG measurements for both compounds. For instance, once the power density of the laser emitter increased to ≥ 20 mW/cm², the powder was burned from white to gray in color, accompanied with the sharp decline of SHG signal. It is well known that the output of SHG signal increases with the enhancement of the input laser energy. Here, the final experimental data were collected by fixing the power density to be 18 mW/cm².

Fig. 6 shows the intensities of the SHG signal of powder BiB₂O₄F and BiB₂O₄(OH) samples as a function of the particle size. It is clear that the SHG intensities increases within the range below 100 μm and then becomes almost independent of the particle size, exhibiting a typical phase-matching behavior, which is consistent with the theoretical anticipation. The further comparison with BIBO sample (105-125 μm , as the reference) reveals that the SHG signals of BiB₂O₄F and BiB₂O₄(OH) are about 2.07 and 0.57 times of BIBO, respectively. Therefore, the experimental d_{powder} are estimated to be 4.72 and 2.48 pm/V, respectively, which are smaller than our calculated values (5.82 and 3.62 pm/V).

It is reasonable that the currently measured d_{powder} are lower than the theoretical values, because the sieved particles for optical measurements are in fact aggregations of smaller crystallites of BiB₂O₄F (see the SEM images as shown in Fig. 2a). We spent months on the hydrothermal synthesis to get large single crystals, however all failed. Nevertheless, the very strong SHG signals, especially for BiB₂O₄F, already validate our original anticipation that they are good NLO materials with much stronger SHG effects than previous reported values.

Here, we should give an explanation why there is such a large difference in SHG efficiency between our results and that in ref. 27. The previous study mainly focused on the structural

chemistry of three bismuth borates and the observable SHG output was only a supporting evidence for the noncentrosymmetric structures. The authors of ref. 27 interpreted that the SHG response might come from the one-dimensional borate chains, like in the case of Pb₆B₁₁O₁₈(OH)₉, which is however not correct (please refer to the discussions below). As mentioned above, both BiB₂O₄F and BiB₂O₄(OH) have a low damage threshold and probably the burning phenomenon was not noticed at that time. We believe this is the major reason why a significant low SHG effect was reported in ref. 27.

In addition, in ref. 27, they report the SHG effect based on a powder sample. We did our best to synthesize crystals. Although we did not obtain perfect and large single crystals for BiB₂O₄F, the average size of the crystals are tens of micrometers (See Fig. 2a). Larger crystals would give stronger SHG signals. This might be the second reason why our experiments gave a higher d_{powder} .

More importantly, we move on to further analyze the structural-property relationship and try to figure out the significance of the incorporation of fluorine, which may have a general instructive effect on finding new NLO materials.

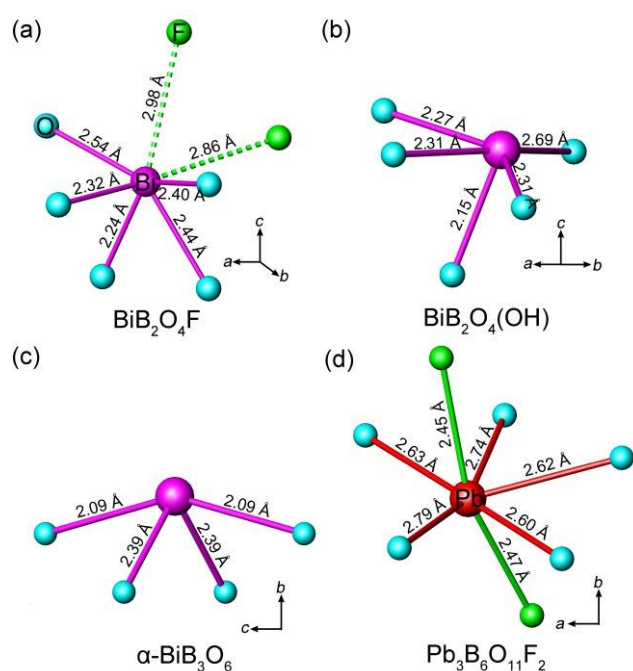
Structure-property relationship

The geometrical sum of the microscopic second-order susceptibility tensors of active units determines the overall SHG coefficient of a crystal. Hence an efficient spatial arrangement of the microscopic groups will generate a relative large macroscopic SHG coefficient. In BIBO, for example, the Bi³⁺ cations bond to the neighbor O²⁻ anions, forming the (BiO₄)⁵⁻ groups with a pyramidal shape,¹² so the Bi 6s lone pair electrons “point” toward the “empty” space along the polar *b*-axis, indicating a strong anisotropy of (BiO₄)⁵⁻ (Fig. 7c). Moreover, the orientation of all (BiO₄)⁵⁻ groups are identical, so

RESEARCH ARTICLE

Table 2 Calculated results and real-space atom-cutting analysis for the nonlinear optical properties in $\text{BiB}_2\text{O}_4\text{F}$ at the incident light wavelength of 1064 nm.

SHG coefficients (pm/V)	Original	Only BO_4	Only BO_3F	Only BiO_5
d_{11}	4.49	0.42	1.48	4.59
d_{16}	2.28	0.31	0.81	1.68
d_{15}	1.44	0.42	-0.07	1.13
d_{33}	-11.60	-0.65	-2.18	-10.91
d_{powder}	5.82	0.57 (10%)	1.50 (26%)	5.59 (96%)
Δn	0.018	0.008	0.014	0.016

Fig. 7 Coordination environments of Bi^{3+} cations in (a) $\text{BiB}_2\text{O}_4\text{F}$, (b) $\text{BiB}_2\text{O}_4(\text{OH})$, (c) $\alpha\text{-BiB}_3\text{O}_6$, and Pb^{2+} cation in (d) $\text{Pb}_3\text{B}_6\text{O}_{11}\text{F}_2$.

their microscopic second-order susceptibility tensors are simply superposed. This leads to the very large overall SHG coefficient for BIBO and the predominant contribution is from $(\text{BiO}_4)^{5-}$ (giving almost 90% of the total value).¹²

Both $\text{BiB}_2\text{O}_4\text{F}$ and $\text{BiB}_2\text{O}_4(\text{OH})$ have a unique polar axis along the c -direction. Figs. 7a and 7b give the coordination environment of Bi^{3+} in $\text{BiB}_2\text{O}_4\text{F}$ and $\text{BiB}_2\text{O}_4(\text{OH})$ respectively, which suggest the $6s$ lone pair electrons are basically aligned along the c -axis. The microscopic second-order susceptibility tensors from BiO_5 groups are canceled out within the ab -plane but have a superposed effect along the polar direction. The interesting question is why these two close-related structures generate largely different NLO responses, i.e. the SHG output of $\text{BiB}_2\text{O}_4\text{F}$ is much stronger than $\text{BiB}_2\text{O}_4(\text{OH})$.

Accordingly, the respective contributions of each ionic groups to the overall optical effects were investigated by adopting the real-space atom-cutting method.⁶ There are two crystallographically independent B atoms in $\text{BiB}_2\text{O}_4\text{F}$, one presents as $[\text{BO}_4]$, and the other is coordinated by three oxygen and one F as $[\text{BO}_3\text{F}]$ (Fig. 1). The bismuth atom is linked to five oxygen atoms by strong Bi-O bonds with the lengths of 2.24–2.54 Å (Fig. 7a). Therefore, the respective contribution of the three anionic groups, i.e., $[\text{BO}_4]$, $[\text{BO}_3\text{F}]$ and $[\text{BiO}_5]$, to the birefringence and SHG coefficients were analyzed, as shown in Table 2. The sums of the contributions from various anionic groups to the optical properties are always larger than the original total values because the oxygen ions were calculated twice in the atom-cutting procedures. It can be seen that the $[\text{BiO}_5]$ and $[\text{BO}_3\text{F}]$ groups are the main contributors for the birefringence, and the contributions are comparable.

For the contribution of SHG coefficients, one may easily find that the $[\text{BiO}_5]$ groups have the dominant contribution (giving ~96% of the total value) in $\text{BiB}_2\text{O}_4\text{F}$, which is similar with the situation of BIBO. Since $\text{BiB}_2\text{O}_4\text{F}$ and $\text{BiB}_2\text{O}_4(\text{OH})$ have the similar spatial arrangement of $[\text{BiO}_5]$ and borate groups (see Fig. 1), the substitution of OH^- by F^- should be responsible for the stronger SHG output of $\text{BiB}_2\text{O}_4\text{F}$. First, the contribution to the total NLO response of $[\text{BO}_3\text{F}]$ groups (~26%) is larger than that of $[\text{BO}_4]$ groups (~10%) in $\text{BiB}_2\text{O}_4\text{F}$, because $[\text{BO}_3\text{F}]$ tetrahedron exhibits a larger spatial anisotropy due to the partial substitution of O atoms by F atoms. More importantly, the presence of F also influences the surrounding environment of Bi^{3+} . As shown in Fig. 7a, two F atoms were found both above Bi^{3+} with distances of 2.86 and 2.98 Å. Fluorine is the most electronegative atom, therefore, the non-bonding electrons ($6s^2$ electrons) of Bi^{3+} can be withdrawn towards two F atoms (along the c -axis) and therefore leading to a higher local polarization, which is beneficial to enhance the total SHG response.

There also exists another interesting noncentrosymmetric lead borate, $\text{Pb}_3\text{B}_6\text{O}_{11}\text{F}_2$,¹⁹ which exhibits a SHG response arisen from the superposing effects of the borate groups and the distorted $[\text{PbO}_x\text{F}_2]$ ($x = 4-6$) polyhedra. The presence of F also

affects the stereotactic chemistry of Pb^{2+} . However, the F-Pb-F angles are $\sim 160^\circ$ (Fig. 7d), then majority of their electron-withdrawing effects on the lone pair electrons of Pb^{2+} are neutralized, so only a moderate SHG response was observed. Then, look back into the case in $\text{BiB}_2\text{O}_4\text{F}$, these two F atoms locate at the same side of Bi (the F-Bi-F angle is $\sim 70^\circ$), indicating their electron-withdrawing effects are synergistic. And it leads to a superior performance of $\text{BiB}_2\text{O}_4\text{F}$ comparing to $\text{BiB}_2\text{O}_4(\text{OH})$.

BIBO is the star compound in borate NLO materials,^{12,32} which was used as the reference of SHG signals in our study. From the structural viewpoint, the strong SHG effect for BIBO originates from the perfect spatial arrangement of $[\text{BiO}_4]$ groups.¹² In our study, the powder SHG effect of $\text{BiB}_2\text{O}_4\text{F}$ is about two times of that in BIBO, according to either theoretical or experimental results. As discussed above, the incorporation of fluorine in $\text{BiB}_2\text{O}_4\text{F}$ leads to a synergistic increase of local polarizations of $[\text{BiO}_5]$ and $[\text{BO}_3\text{F}]$, and hence a very strong NLO response. In addition, the spatial density of the $[\text{BiO}_5]$ groups in $\text{BiB}_2\text{O}_4\text{F}$ is about 1.33 times denser than that of the $[\text{BiO}_4]$ groups in BIBO.

Conclusion

In literature, there are numerous metal borates showing excellent UV NLO properties. Most studies are devoted to those materials with appropriate arrangements of polar structure units, which already become the fundamental principle for NLO materials. Here in our work, we rationalize the additional function of fluorine, which is the most electronegative atom, on further enhancing the SHG efficiency by withdrawing lone pair electrons of Bi^{3+} . In view of this, we re-investigated the SHG property of a unique bismuth borate, $\text{BiB}_2\text{O}_4\text{F}$, where F coordinates to both B and Bi atoms. DFT calculations and experimental results both point to a very strong d_{powder} , even higher than the star compound BIBO. Our detailed analyses on structure-property relationship, especially the comparison study with its relative compound $\text{BiB}_2\text{O}_4(\text{OH})$, validate our judgement on the functionality of F atoms, which may have a general instructive effect on finding new NLO materials.

Acknowledgements

This work was supported by the Nature Science Foundation of China (Grants 21101175, 21171178, 91222106, 91022036 and 11174297) and National Basic Research Project of China (Grants 2010CB630701 and 2011CB922204). We acknowledge Prof. Z. G. Hu (Technical Institute of Physics and Chemistry, Chinese Academy of Science) for the assistance on the SHG measurements.

Notes and references

^a College of Chemistry and Chemical Engineering, Chongqing University, Chongqing 400044, People's Republic of China. Email: congrihong@cqu.edu.cn, taoyang@cqu.edu.cn; Tel: +86-23-65105065.

^b Beijing Center for Crystal R&D, Key Lab of Functional Crystals and Laser Technology, Technical Institute of Physics and Chemistry, Chinese Academy of Science, P.O. Box 2711, Beijing 100080, People's Republic of China. Email: zslin@mail.ipc.ac.cn.

^c University of Chinese Academy of Sciences, Beijing 100049, People's Republic China.

Electronic Supplementary Information (ESI) available: Computational methods, tables of crystallographic data, TG curve and SEM photo for $\text{BiB}_2\text{O}_4(\text{OH})$, powder XRD patterns for both $\text{BiB}_2\text{O}_4(\text{OH})$ and $\text{BiB}_2\text{O}_4\text{F}$. See DOI: 10.1039/b000000x/

1. P. Becker, *Adv. Mater.*, 1998, **10**, 979-992.
2. C. Chen, Z. Lin, Z. Wang, *Appl. Phys. B*, 2005, **80**, 1-25.
3. F. Li, X. L. Hou, S. L. Pan, *Chem. Mater.*, 2009, **21**, 2846-2850.
4. P. Shiv Halasyamani, K. R. Poeppelmeier, *Chem. Mater.*, 1998, **10**, 2753-2769.
5. C. F. Sun, C. L. Hu, J. G. Mao, *Chem. Commun.*, 2012, **48**, 4220-4222.
6. J. Lin, M. H. Lee, Z. P. Liu, C. T. Chen, C. J. Pickard *Phys. Rev. B*, 1999, **60**, 13380-13389.
7. Z. S. Lin, J. Lin, Z. Z. Wang, C. T. Chen, *Phys. Rev. B*, 2000, **62**, 1757-1764.
8. H. S. Ra, K. M. Ok, P. Shiv Halasyamani, *J. Am. Chem. Soc.*, 2003, **125**, 7764-7765.
9. E. O. Chi, K. M. Ok, Y. Porter, P. Shiv Halasyamani, *Chem. Mater.*, 2006, **18**, 2070-2074.
10. Y. Inaguma, M. Yoshida, T. Katsumata, *J. Am. Chem. Soc.*, 2008, **130**, 6704-6705.
11. W. L. Zhang, W. D. Cheng, H. Zhang, L. Geng, C. S. Lin, Z. Z. He, *J. Am. Chem. Soc.*, 2010, **132**, 1508-1509.
12. Z. S. Lin, Z. Z. Wang, C. T. Chen, M. H. Lee, *J. Appl. Phys.*, 2001, **90**, 5585-5590.
13. S. H. Kim, J. Yeon, P. Shiv Halasyamani, *Chem. Mater.*, 2009, **21**, 5335-5342.
14. F. Kong, S. P. Huang, Z. M. Sun, J. G. Mao, W. D. Cheng, *J. Am. Chem. Soc.*, 2006, **128**, 7750-7751.
15. Y. Z. Huang, L. M. Wu, X. T. Wu, L. H. Li, L. Chen, Y. F. Zhang, *J. Am. Chem. Soc.*, 2010, **132**, 12788-12789.
16. H. P. Wu, S. L. Pan, K. R. Poeppelmeier, H. Y. Li, D. Z. Jia, Z. H. Chen, X. Y. Fan, Y. Yang, J. M. Rondinelli, H. S. Luo, *J. Am. Chem. Soc.*, 2011, **133**, 7786-7790.
17. B. C. Wu, D. Y. Tang, N. Ye, C. T. Chen, *Opt. Mater.*, 1996, **5**, 105-109.
18. Z. S. Lin, Z. Z. Wang, C. T. Chen, S. K. Chen, M. H. Lee, *Chem. Phys. Lett.*, 2003, **367**, 523-527.
19. H. Y. Li, H. P. Wu, X. Su, H. W. Yu, S. L. Pan, Z. H. Yang, Y. Lu, J. Han, K. R. Poeppelmeier, *J. Mater. Chem. C*, 2014, **2**, 1704-1710.
20. G. H. Zou, L. Y. Zhang, N. Ye, *CrystEngComm*, 2013, **15**, 2422-2427.
21. D. M. Chackraburty, *Acta Crystallogr.*, 1957, **10**, 199-200.
22. G. Cakmak, T. Pilz, M. Z. Jansen, *Anorg. Allg. Chem.*, 2012, **638**, 1411-1415.
23. T. Pilz, M. Z. Jansen, *Anorg. Allg. Chem.*, 2011, **637**, 2148-2152.
24. T. Pilz, H. Nuss, M. Jansen, *J. Solid State Chem.*, 2012, **186**, 104-108.
25. G. Cakmak, J. Nuss, M. Jansen, *Z. Anorg. Allg. Chem.*, 2009, **635**, 631-636.
26. B. Andriyevsky, T. Pilz, J. Yeon, P. Shiv Halasyamani, K. Doll, M. Jansen, *J. Phys. Chem. Solids*, 2013, **74**, 616-623.

27. L. Y. Li, G. B. Li, Y. X. Wang, F. H. Liao, J. H. Lin, *Chem. Mater.*, 2005, **17**, 4174-4180.
28. M. C. Payne, M. P. Teter, D. C. Allan, T. A. Arias, J. D. Joannopoulos, *Rev. Mod. Phys.*, 1992, **64**, 1045-1097.
29. S. J. Clark, M. D. Segall, C. J. Pickard, P. J. Hasnip, M. J. Probert, K. Refson, M. C. Payne, *Zeitschrift Fur Kristallographie*, 2005, **220**, 567-570.
30. S. K. Kurtz, T. T. Perry, *J. Appl. Phys.*, 1968, **39**, 3798-3813.
31. G. M. Sheldrick, SHELXS 97, Program for the Solution of Crystal Structures, and SHELXL 97, Program for the Refinement of Crystal Structures; University of Göttingen: Göttingen, Germany, 1997.
32. H. Hellwig, J. Liebertz, L. Bohatý, *Solid State Commun.*, 1999, **109**, 249-251.